Reconfigurable source illusion device for airborne sound using an enclosed adjustable piezoelectric metasurface

Yi-Fan Tang(唐一璠) and Shu-Yu Lin(林书玉)†

Shaanxi Key Laboratory of Ultrasonics, Institute of Applied Acoustics, Shaanxi Normal University, Xi'an 710119, *China*

(Received 14 September 2022; revised manuscript received 1 November 2022; accepted manuscript online 3 November 2022)

Source illusion is an important issue in acoustic fields that has significant applications in various practical scenarios. Recent progress in acoustic metasurfaces has broken the limitation of manipulating large-scale waves at subwavelength scales and enables a better illusion capability, while there is still a problem that most previous studies are hampered by a lack of tuning capability. Here we propose a reconfigurable source illusion device capable of providing azimuthally-dependent phase delay in real-time via changing the static voltage distribution. The resulting device is implemented by employing an adjustable piezoelectric metasurface with a subwavelength thickness that can achieve a full 2π-phase shift while maintaining efficient transmittance. The effectiveness of our mechanism is demonstrated via two distinctive source illusion phenomena of shifting and transforming a simple point source without changing the device geometry. We anticipate that our methodology, which does not require a large device size or a complicated phased array, will open up new avenues for the miniaturization and integration of source illusion devices and may promote their on-chip applications in a variety of fields, such as acoustic camouflage and manipulation precision.

Keywords: acoustic metasurface, source illusion, piezoelectric materials, adjustable control

PACS: 43.20.+g, 43.40.+s, 43.90.+v, 52.35.Dm **DOI:** 10.1088/1674-1056/ac9fc0

1. Introduction

The past decades have witnessed the rapid development of the invisibility cloak capable of canceling the scattering effect from electromagnetic signals[1–6] to acoustical signals.[7–10] A family of more general invisibility cloaks has been implemented by employing the technique of coordinate transformation that can convert the physical system into an illusion system.[11–13] These required material parameters are usually anisotropic[14] and inhomogeneous,[15] which were not readily available until the recent advent of metamaterials. Metasurfaces, as a special kind of metamaterial with a reduced dimension, help to freely manipulate the wavefront to yield novel phenomena such as anomalous refraction and reflection,[16–19] stable vortex beams,[20–23] high-quality holograms,[24–26] and invisibility cloaks.[27–29] Unlike the conventional invisibility cloak that can simply cancel the scattered field produced by an object, the emergence of the illusion cloak can freely manipulate the scattered field as if the object is changed into another object of one's choice.[30] The material parameters of the illusion cloak require negative index materials[31] and their spatial distributions should be connected with the original object.[32] The first experimentally verified acoustic illusion cloak is simply made of positive-index anisotropic materials whose parameters are independent of either the boundary or the object.[33] Subsequently, a three-dimensional acoustic cloak that allows the concealing of arbitrary objects located inside an open cavity with arbitrary boundaries was reported.[34] The aforementioned acoustic illusions can manipulate the pressure field distribution scattered by an object as illuminated by the external field. Until recently, a theoretical framework and experimental realization of a source illusion device to manipulate flexural waves using elastic metasurfaces were demonstrated.[35] The concept of source illusion for airborne sound was proposed to realize intriguing illusion phenomena, which are implemented by acoustic metasurfaces to provide azimuthally-dependent phase delay.[36] However, the proposed source illusion devices can only have a fixed functionality once fabricated, which means it is hampered by a lack of tuning capability. Driven by the development of adjustable acoustic metasurfaces, piezoelectric materials were introduced into acoustic metasurfaces to increase adjustability. Moreover, the mechanism for designing the source illusion device can freely manipulate the wavefront of the transmitted wave in real time via reconfiguring the voltage distribution. It can be expected that the realization of the reconfigurable source illusion for airborne sound would be highly desired in practical applications ranging from architectural design to ultrasound imaging.

In this work, we introduce piezoelectric materials into the design of the source illusion device to realize a reconfigurable airborne source illusion device and provide an azimuthally-dependent phase delay in real time via changing the static voltage distribution. The underlying mechanism of the adjustable piezoelectric metasurface is that the stresses introduced by the static voltage exerted on the piezoelectric layers break the tension balance of the hybrid membrane structure to

†Corresponding author. E-mail: sylin@snnu.edu.cn

© 2023 Chinese Physical Society and IOP Publishing Ltd

generate bending deformation, resulting in the static voltage as a function of the phase shift of the transmitted wave. As a consequence, the resulting device can realize versatile illusion phenomena by reconfiguring the static voltage distribution without changing the device geometry. We demonstrate two distinctive source illusion effects of source shifter and source converter via numerical simulations, which will help to offer a new design methodology in practical applications.

2. Model and mechanism

The schematic diagram of our proposed mechanism for generating a source illusion device for airborne sound is illustrated in Figs. 1(a) and 1(b). Figure 1(a) illustrates the target wave profile characterized by the phase profile $\phi_t(x,y)$ regardless of the amplitude profile. If we have an original source whose phase profile is $\phi_o(x,y)$, the enclosed adjustable piezoelectric metasurface with the phase discontinuity of $\phi_t(x,y)-\phi_o(x,y)$ will change the original incident field into an arbitrary target profile. The gap between the piezoelectric metasurface unit cells is not connected with the outside world. In the numerical simulation, we enclose the gap with a hard-plastic plate. Since the characteristic acoustic impedance of the hard-plastic plate is much higher than that of the air, the gap between the unit cells of the piezoelectric metasurface has almost no influence on the sound field. Figure 1(c) shows the zoom-in view of the unit cell of the piezoelectric metasurface, which is composed of a fourlayer identical hybrid membrane structure. The red arrow represents the incident waves and the green arrow stands for transmitted waves, respectively. The configuration of an individual hybrid membrane structure formed by depositing four piezoelectric patches on the upper and lower sides of the membrane with small steel attached to its center is depicted in Fig. 1(d). For each piezoelectric patch, an electric circuit is attached to exert a static voltage load between the two surfaces in a controlled manner. Due to the piezoelectric effect, the stress of the piezoelectric patches is induced by the applied static voltage, which breaks the tension balance of the piezoelectric patches. Thereby the equal but opposite voltages on the two layers of the piezoelectric patches will generate bending deformation due to the extension of one side and the contraction of the other side. This enables simple manipulation of the propagation phase of the acoustic wave after passing through the proposed unit cell by adjusting the electric potential of circuit. Here, the piezoelectric patch is made of PZT-5H material and polarized in the thickness direction. The middle layer of the hybrid membrane structure is a low-density polyethylene membrane whose length L_2 and thickness d_2 are chosen as 40 mm and 0.2 mm, respectively. The small steel, with a length L_1 of 2.5 mm and a thickness d_1 of 0.5 mm, is to tune the vibrational eigenmodes of the membrane. On the upper and lower sides of the membrane, we use four piezoelectric patches whose length L_3 is 5 mm. The distance between two identical hybrid membrane structures is 80 mm. The mass density of the piezoelectric material is 7750 kg/m^3. The density, Young's modulus, and Poisson's ratio are 1420 kg/m^3, 2.5 GPa, and 0.34 for the membrane, and 7850 kg/m^3, 205 GPa, and 0.28 for small steel, respectively. The damping of the membrane and the mechanical loss of the piezoelectric patches are both 0.001. The unit cell of the proposed piezoelectric metasurface is expected to control the phase of the transmitted waves in a controlled manner by switching the static voltage distribution without changing the device geometry.

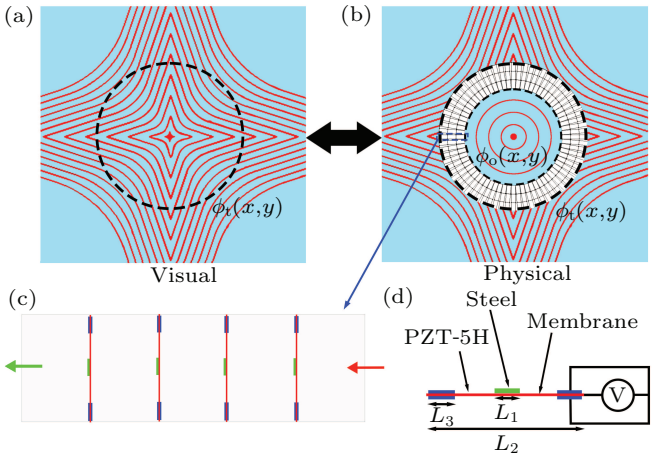


Fig. 1. (a) The target wave profile characterized by the phase profile $\phi_t(x,y)$ produced by a complicated source. (b) The schematic diagram of making illusion implemented by an enclosed adjustable piezoelectric metasurface (between the two black dashed circles). The primitive unit cell outlined by the blue dotted box. (c) The zoom-in view of the unit cell of our proposed adjustable piezoelectric metasurface. (d) The configuration of an individual hybrid membrane structure of the unit cell.

Throughout the paper, the numerical simulations are performed by the finite element method based on the Pressure Acoustics Module, Solid Mechanics Module, and Electrostatics Module of COMSOL MULTIPHYSICS. First, we use the steady-state solver to calculate the steady-state results of the piezoelectric metasurface unit cell after applying a static voltage under the coupling of the Solid Mechanics Module and Electrostatics Module. Then we choose the linear perturbation solver to calculate the transmission coefficient and phase shift of the piezoelectric metasurface unit cell under the Pressure Acoustics Module. The plane wave radiation boundary is imposed on the two ends of the cylindrical waveguide to eliminate reflected waves, while the incident wave is only excited at the right side. Figure 2(a) demonstrates the transmission coefficient (blue line) and phase shift (red line) as a function of the frequency, where three resonance peaks marked by the black dots can be observed in the spectrum. It is worth stressing that we elaborately designed the distance between two hybrid membrane structures to realize the near-unity transmission efficiency while maintaining a smooth phase shift. The introduced small steel is capable of adjusting the eigenfrequency

of the unit cell. Figure 2(b) shows the corresponding cross-section view of the total displacement field of the unit cell at the first, second, and third resonance frequencies. The first, second, third, and fourth layers of the unit cell are represented by i, ii, iii, and iv in Fig. 2(b) respectively. The first eigenmode of the unit cell is characterized by the in-phase oscillation (dipolar resonance) of layers i and ii and the out-of-phase oscillations (monopolar resonance) of the layers iii and iv at the frequency of $f_1 = 981.4$ Hz. Here, the two groups of the hybrid membrane structures are regarded as a whole and described as monopole or dipole, respectively. The vibration amplitude of the hybrid membrane structures in each group does not need to be equal because the resonance modes of the piezoelectric metasurface cell are formed by the synergy of the four-layer hybrid membrane structures. The second eigenmode of the unit cell is featured by the monopolar resonance of the layers i and iii at the frequency of $f_2 = 1011$ Hz. Similarly, the third eigenmode occurs at the frequency of $f_3 = 1044$ Hz characterized by the monopolar resonance of layers i and ii and dipolar resonance of the layers i and iii, respectively.[37,38] There is almost no vibration in layer iv at this frequency, indicating that the third eigenmode is formed by the synergy of the first three layers of the hybrid membrane structures. Instead of employing the technique of coordinate transformation, our mechanism uses an enclosed piezoelectric metasurface to produce an azimuthally-dependent phase delay while maintaining high transmittance, making a phase shift of the transmitted wave dependence of the value of electric potential. In the current study, we chose the third resonance frequency to demonstrate the functionality of our scheme. The phase shift (cyan line) and transmission coefficient (magenta line) of the transmitted wave dependence of input static voltage are plotted in Fig. 2(c) at the resonance frequency of 1044 Hz. For the sake of simplicity, it is competent to select the values of electric potential for eight units that can cover the 2π span with a discrete phase step of $\pi/4$, as marked by the eight black dots. The propagation of incident waves has been delayed after passing through the unit cells as shown in Fig. 2(d), where the peak of the pressure field can shift up to a wavelength. The corresponding static voltage induces the eight discrete cell units to generate phase delay shifted from to 2π with the near-unity transmission efficiency at the working frequency. In what follows, we will display the adjustability of our proposed adjustable piezoelectric metasurface to realize the source illusion phenomenon in real time by modulating the voltage distribution.

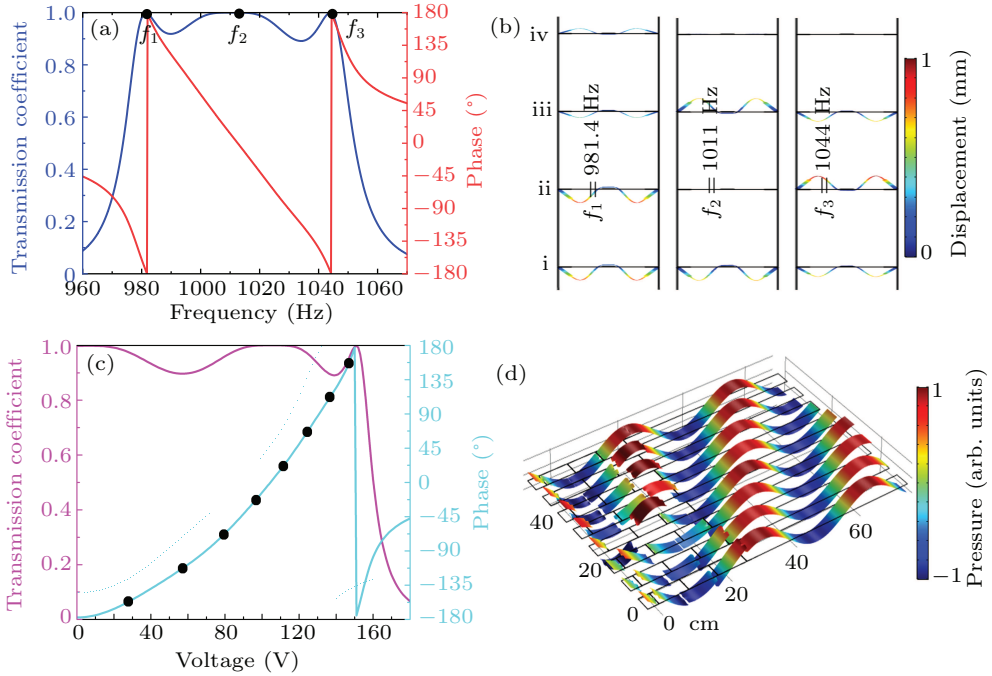


Fig. 2. (a) The simulated frequency dependence of the transmission coefficient (blue line) and phase shift (red line) for the unit cell with three resonance peaks at f_1, f_2, and f_3, respectively. (b) Cross-section view of the total displacement fields for the first, second, and third eigenmodes at the three resonance frequencies. The first, second, third, and fourth layers of the unit cell are represented by i, ii, iii, and iv. (c) The phase shift (cyan line) and transmission coefficient (magenta line) of the transmitted waves as a function of static voltage. Black dots: eight discrete units needed for realizing the desired phase delay. (d) The acoustic pressure strips of the transmitted waves by eight discrete unit cells.

3. Results and discussion

First, we will exemplify the performance of our enclosed adjustable piezoelectric metasurface to realize a source shifter capable of virtually moving the location of the source by a certain distance. The schematic of the conversion process is depicted in Fig. 3(a), where the blue dot stands for the physical source which is the actual source and the black dashed circle represents the visual source, respectively. For simplicity without losing generality, we focus on a case where a physical

source at origin (0, 0) is shifted to a virtual source at (x_s, y_s). The azimuthal distribution of the phase profile should satisfy the following equation:[29]

$$\phi(\theta) = \frac{2\pi}{\lambda}(r_1 - r), \tag{1}$$

where $r_1 = \sqrt{(r\cos\theta - x_s)^2 + (r\sin\theta - y_s)^2}$, λ is the wavelength, r is the radius of the enclosed adjustable piezoelectric metasurface, and θ is the azimuthal angle. For given $r = 4.5\lambda/\pi$, $x_s = 0$, and $y_s = 0.7\lambda$, the discrete phase shift profile anticipated by Eq. (1) (red dot line) and the corresponding applied static voltage profile (blue dot line) provided by the piezoelectric metasurface as a function of azimuthal angle are plotted in Fig. 3(b). Figure 3(c) shows the simulated pressure field distribution of the source shifter implemented by the enclosed piezoelectric metasurface at the operating frequency. Inside the source illusion device, the physical source radiates the cylindrical sound waves, while the pressure field remains the cylindrical form outside the illusion device with a symmetry center located at (0, 0.7λ). More interestingly, when we put the physical source at (0, -0.7λ), it can be seen that the source radiates acoustic energy omnidirectionally into all directions at the location of (0, 0), as schematically depicted in Fig. 3(d). Figure 3(e) demonstrates the simulated pressure field distribution for the particular case, $y_s = -0.7\lambda$, where the common center is found at the origin and the radiated field generated by the source shifter verifies the theoretical prediction. The resultant wavefront has small ripples outside the illusion device which can be implemented by employing optimized or smaller unit cells to reduce the multiple reflections.[29]

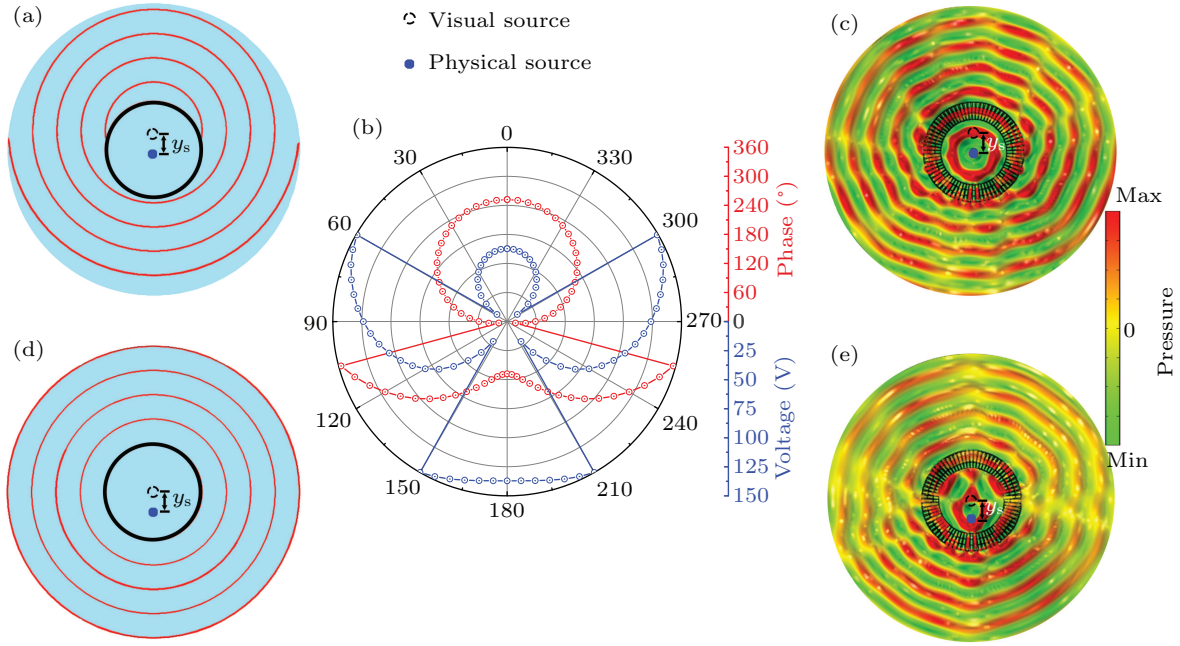


Fig. 3. (a) Schematic diagram of the design for generating source shifter. The black dashed circle represents the visual source and the blue dot stands for the physical source. (b) The discrete phase shift profile anticipated by Eq. (1) (red dot line) and the corresponding applied static voltage profile (blue dot line) provided by the piezoelectric metasurface versus azimuthal angle. (c) The simulated normalized pressure field for source shifter implemented by the adjustable piezoelectric metasurface. (d)–(e) The schematic diagram and simulated normalized pressure field of the source shifter, the source is placed at (0, -0.7λ).

To further illustrate the flexibility of our enclosed adjustable piezoelectric metasurface, we demonstrate that the pattern of the radiated field of a point source can be converted to another complicated pattern by reconfiguring the voltage distribution. Figure 4(a) shows the schematic diagram of a helical wave generator that can impart orbital angular momentum to a point source. To this end, the desired phase profile is employed on the metasurface and the phase $\phi(\theta)$ imposed at every point along the azimuthal direction must satisfy the following equation:[30]

$$\phi(\theta) = M\theta + \frac{2\pi}{\lambda}\left(r_2 + \sqrt{x^2 + y^2} - r\right) + \phi_0, \tag{2}$$

where $r_2 = \sqrt{(r\cos\theta - x_0)^2 + (r\sin\theta - y_0)^2}$ and M is the additional angular momentum, (x_0, y_0) represents the location of the physical source, and the ϕ_0 refers to the initial phase. The discrete phase shift profile acquired by Eq. (2) (red dot line) and the corresponding static voltage profile (blue dot line) supported by the adjustable piezoelectric metasurface are depicted in Fig. 4(b), where the parameters are chosen as $M = 6$, $(x_0, y_0) = (0, 0)$, and $\phi_0 = 0$. By changing the spatial distribution of the voltage in Fig. 3(b), it is convenient to convert the above source shifter to a source converter for generating an illusion effect. It is observed that the radiated field from a point source has a spiral wavefront after passing through the proposed illusion device, as depicted in Fig. 4(c). In the numerical simulation, a single point source emits cylindrical

acoustic waves from the center, and perfectly matched layers are applied at the outer boundary to absorb the obliquely incident waves. The cylindrical wave transforms into a spiral wave with 6 branches, implying that the phase undergoes 12π change in an annular loop. In another case, if we put the location of the physical source at $(0, -0.7\lambda)$ instead of $(0, 0)$, the schematic diagram of the conversion process is demonstrated in Fig. 4(d). We calculated the discrete phase shift profile and the static voltage distribution as a function of azimuthal angle and plotted the results in Fig. 4(e). Figure 4(f) shows the normalized pressure field distribution, which agrees well with the idealized design, proving that our proposed scheme can convert the cylindrical wave into a spiral wave.

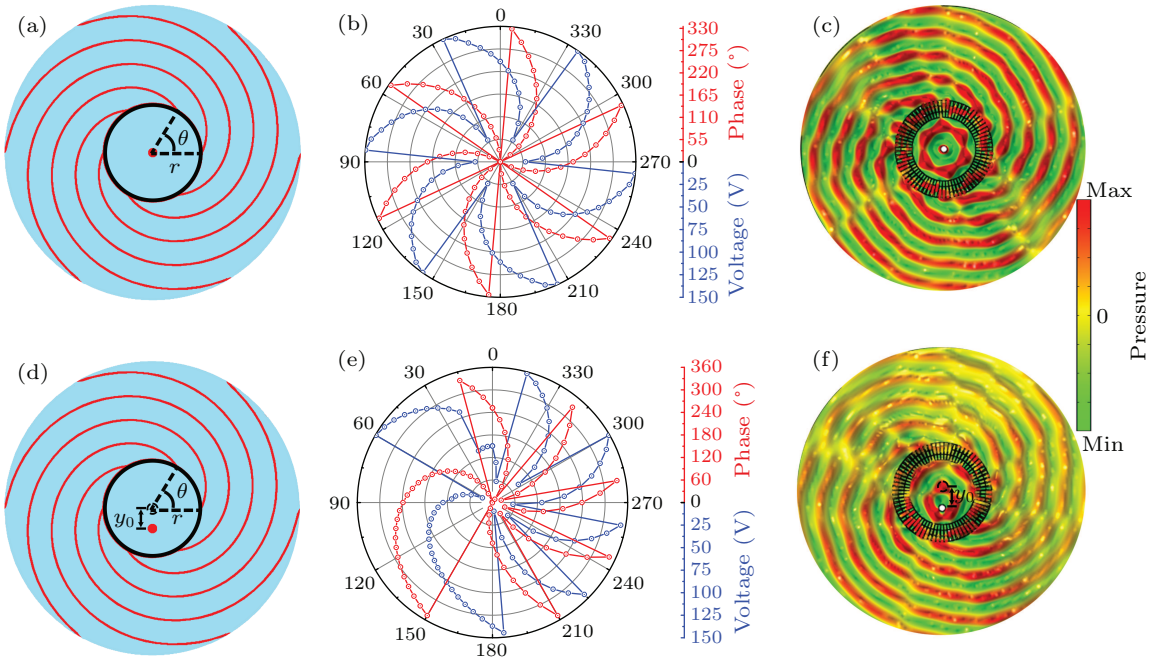


Fig. 4. (a) Schematic diagram of the design for generating a source converter. (b) The discrete phase shift profile (red dot line) and the applied static voltage profile (blue dot line) versus azimuthal angle. (c) The simulated normalized pressure field of the source converter implemented by the adjustable piezoelectric metasurface. (d)–(e) The schematic diagram, discrete phase shift profile, voltage distribution, and simulated normalized pressure field of the source converter, the source is placed at $(0, -0.7\lambda)$.

4. Conclusions

In summary, the previous acoustic illusions can manipulate the pressure field distribution scattered by an object as illuminated by the external field, which needs to rely on transformation acoustics techniques. Our proposed enclosed adjustable piezoelectric metasurface can directly produce an acoustic illusion for an airborne sound source itself. The resulting device is realized by an enclosed adjustable piezoelectric metasurface capable of producing a desired discontinuity phase along the azimuthal direction. The underlying mechanism of the resulting device is that the stresses introduced by the static voltage exerted on the piezoelectric layers break the tension balance of the hybrid membrane structure to generate bending deformation, resulting in the static voltage as a function of the phase shift of the transmitted wave. The residual stress of the membranes may become an annoying issue, so we need to test the acoustic properties of each hybrid membrane structure and choose four hybrid membrane structures with the same acoustic properties to form a piezoelectric metasurface unit cell. The experiment can be implemented with difficulty because we have to ensure the consistency of the hybrid membrane structures and the high precision of the sample in the experiment process. Although the thickness of our proposed piezoelectric metasurface is not at a deep subwavelength scale, the enclosed piezoelectric metasurface in the simulation can virtually realize two distinctive source illusion phenomena of shifting and transforming a simple point source. The next step of our work is to achieve the unit cell with a deep subwavelength scale to eliminate the difference between the inner and outer cross-sectional areas and make its experimental realization. The resulting device can realize the source shifter and source converter by reconfiguring the DC voltage distribution without changing the device geometry. Our design may find important uses in a great variety of scenarios that demand special manipulations of the radiation field such as in acoustic communication, architectural acoustics, and acoustic camouflage.

Acknowledgements

Project supported by the National Natural Science Foundation of China (Grant Nos. 12174240, 11674206, and 11874253) and the Natural Science Basic Research Plan in the

Shaanxi Province of China (Grant No. 2023-JC-QN-0049).

References

[1] Landy N and Smith D R 2013 *Nat. Mater.* **12** 25
[2] Gharghi M, Gladden C, Zentgraf T, Liu Y, Yin X, Valentine J and Zhang X 2011 *Nano Lett.* **11** 2825
[3] Valentine J, Li J, Zentgraf T, Bartal G and Zhang X 2009 *Nat. Mater.* **8** 568
[4] Schurig D, Mock J J, Justice B J, Cummer S A, Pendry J B, Starr A F and Smith D R 2006 *Science* **314** 977
[5] Leonhardt U 2006 *Science* **312** 1777
[6] Pendry J B, Schurig D and Smith D R 2006 *Science* **312** 1780
[7] Popa B I, Zigoneanu L and Cummer S A 2011 *Phys. Rev. Lett.* **106** 253901
[8] Tang Y F, Liang B, Yang J, Yang J and Cheng J C 2019 *Appl. Phys. Express* **12** 064501
[9] Zigoneanu L, Popa B I and Cummer S A 2014 *Nat. Mater.* **13** 352
[10] Torrent D and Sánchez-Dehesa J 2008 *New J. Phys.* **10** 063015
[11] Chen H, Chan C T and Sheng P 2010 *Nat. Mater.* **9** 387
[12] Lai Y, Chen H, Zhang Z Q and Chan C T 2009 *Phys. Rev. Lett.* **102** 093901
[13] Wei Q, Cheng Y and Liu X J 2012 *Phys. Rev. B* **86** 024303
[14] Cummer S A, Popa B I, Schurig D, Smith D R, Pendry J, Rahm M and Starr A 2008 *Phys. Rev. Lett.* **100** 024301
[15] Zhang S, Xia C and Fang N 2011 *Phys. Rev. Lett.* **106** 024301
[16] Li Y, Liang B, Gu Z M, Zou X Y and Cheng J C 2013 *Sci. Rep.* **3** 2546
[17] Jiang X, Li Y, Liang B, Cheng J C and Zhang L 2016 *Phys. Rev. Lett.* **117** 034301
[18] Liu Y, Li Y F and Liu X Z 2019 *Chin. Phys. B* **28** 024301
[19] Chen X, Liu P, Hou Z and Pei Y 2017 *Appl. Phys. Lett.* **110** 161909
[20] Zhu X F, Liang B, Kan W, Zou X and Cheng J C 2011 *Phys. Rev. Lett.* **106** 014301
[21] Jiang X, Liang B, Cheng J C and Qiu C W 2018 *Adv. Mater.* **30** 1800257
[22] Wang W, Liu J J, Liang B and Cheng J C 2022 *Chin. Phys. B* **31** 094302
[23] Jia Y, Zhu Y, Ma C, Cheng Y, Wu D, Deng M and Liu X J 2021 *Phys. Rev. B* **103** 184107
[24] Zhu Y F, Hu J, Fan X, Yang J, Liang B, Zhu X F and Cheng J 2018 *Nat. Commun.* **9** 1632
[25] Tian Y, Wei Q, Cheng Y and Liu X J 2017 *Appl. Phys. Lett.* **110** 191901
[26] Gu Y, Cheng Y and Liu X J 2015 *Appl. Phys. Lett.* **107** 133503
[27] Ni X, Wong Z J, Mrejen M, Wang Y and Zhang X 2015 *Science* **349** 1310
[28] Cheng Y, Yang F, Xu J Y and Liu X J 2008 *Appl. Phys. Lett.* **92** 151913
[29] Gu Y, Cheng Y, Wang J and Liu X J 2015 *J. Appl. Phys.* **118** 024505
[30] Pendry J 2009 *Nature* **460** 579
[31] Lai Y, Ng J, Chen H, Han D, Xiao J, Zhang Z Q and Chan C T 2009 *Phys. Rev. Lett.* **102** 253902
[32] Jiang W X and Cui T J 2011 *Phys. Rev. E* **83** 026601
[33] Kan W W, Liang B, Zhu X F, Li R Q, Zou X, Wu H, Yang J and Cheng J C 2013 *Sci. Rep.* **3** 1427
[34] Kan W W, Liang B, Li R Q, Jiang X, Zou X Y, Yin L L and Cheng J C 2016 *Sci. Rep.* **6** 36936
[35] Liu Y Q, Liang Z X, Liu F, Diba O, Lamb A and Li J 2017 *Phys. Rev. Lett.* **119** 034301
[36] Fan X D, Liang B, Yang J and Cheng J C 2019 *Sci. Rep.* **9** 1750
[37] Yang M, Ma G, Yang Z and Sheng P 2013 *Phys. Rev. Lett.* **110** 134301
[38] Ma F Y, Huang M, Xu Y C and Wu J H 2018 *J. Appl. Phys.* **123** 35104